

Detecting baryon acoustic oscillations by 3d weak lensing

Alessandra Grassi^{*} and Björn Malte Schäfer

Zentrum für Astronomie der Universität Heidelberg, Philosophenweg 12, 69120 Heidelberg, Germany

6 March 2013

ABSTRACT

We investigate the possibility of detecting baryon acoustic oscillation features in the cosmic matter distribution by 3d weak lensing. Baryon oscillations are inaccessible even to weak lensing tomography because of wide line-of-sight weighting functions and require a specialized approach via 3d shear estimates. We quantify the uncertainty of estimating the matter spectrum amplitude at the baryon oscillations wave vectors by a Fisher-matrix approach with a fixed cosmology and show in this way that future weak lensing surveys such as EUCLID and DES are able to pick up the first four wiggles, with EUCLID giving a better precision in the measurement. We also provide a detailed investigation of the correlation existing between errors and of their scaling behavior with respect to survey parameters such as median redshift, error on redshift, error on the galaxy shape measurement, sky coverage, and finally with respect to the number of wiggles one is trying to determine.

Key words: cosmology: large-scale structure, gravitational lensing, methods: analytical

1 INTRODUCTION

Baryon acoustic oscillation (BAO) features are modulations in the cosmic matter distribution on very large spatial scales of roughly ~ 100 Mpc/ h (for a review, see [Bassett & Hlozek 2010](#)). These BAOs are the imprint of oscillations of the photon-baryon fluid in the early universe on the matter density field driven by gravity and the equation of state providing a restoring force, and they are observable in two primary channels: through the observation of anisotropies in the cosmic microwave background (CMB) and through galaxy surveys. The most important features such as their spatial scales, their signature in the CMB, their statistical properties, and their dependence on cosmological parameters is very well understood analytically ([Seljak & Zaldarriaga 1996](#); [Hu & Sugiyama 1996](#); [Montanari & Durrer 2011](#); [Sutherland 2012](#)).

Concerning the determination of cosmological parameters, it is a fortunate situation that they are observable at high redshifts through the primary CMB and at much lower redshifts in the galaxy distribution. Due to the fact that BAOs provide a standard yardstick at two different cosmological epochs, it is possible to constrain the density parameters of cosmic fluids and the possible time evolution of their equation of state parameters in a geometric way, breaking degeneracies that may arise if the equations of state of cosmological fluids are allowed to change with time.

CMB observations carried out by the Cosmic Background Explorer (COBE, [Bennett et al. 1994](#); [Wright et al. 1996](#)) first revealed anisotropies in the CMB, but only the Wilkinson Microwave Anisotropy Probe (WMAP, [Hinshaw et al. 2003, 2007](#); [Nolta et al. 2009](#); [Larson et al. 2011](#)) had sufficient angular resolution such that the BAO scale of ~ 100 Mpc/ h could be resolved at a comoving

distance of ~ 10 Gpc/ h , revealing temperature modulations of the CMB of the order $\Delta T/T_{\text{CMB}} \approx 10^{-5}$ at an angular scale of roughly 2° , with subsequent higher harmonics. Likewise, galaxy surveys have now reached sufficient depth and solid angle that BAO features could be detected as modulations of the galaxy density of the order 10% in both radial and transverse directions. With the assumption of a galaxy biasing model, the longest wavelength BAO modes survive nonlinear structure formation to the present epoch ([Meiksin et al. 1999](#)) and will be targeted by future surveys for the precision determination of cosmological parameters ([Dolney et al. 2006](#); [Angulo et al. 2008](#); [Labatie et al. 2012](#)), in particular dark energy ([Seo & Eisenstein 2003](#); [Eisenstein et al. 2007](#)). Both avenues have contributed significantly to the estimation of cosmological parameters and to the selection of most plausible cosmological models.

Specifically, there are quite a number of detection reports with ongoing surveys, for instance with the Sloan Digital Sky Survey (SDSS, [Eisenstein et al. 2005](#); [Padmanabhan et al. 2007](#); [Percival et al. 2007, 2010](#); [Kazin et al. 2010](#); [Padmanabhan et al. 2012](#); [Mehta et al. 2012](#)), the 2-Degree Field Galaxy Redshift Survey (2dFGRS, [Percival et al. 2007](#); [Beutler et al. 2011](#)), the WiggleZ-survey ([Parkinson et al. 2012](#)) and Lyman- α data ([Busca et al. 2012](#)) with subsequent determination of cosmological parameters which confirm spatial flatness and the low matter density found by CMB observations, if flatness is assumed prior to the analysis. Recent studies ([Parejko et al. 2012](#); [Zhao et al. 2012](#)) were able to constrain neutrino masses. BAO modulations have been found as longitudinal as well as transverse modes in the galaxy density ([Gaztañaga et al. 2009](#); [Kazin et al. 2010](#); [Gaztañaga et al. 2009](#)) and their issues of model selection and parameter estimation have been addressed thoroughly ([Cabr  & Gaztañaga 2011](#)).

The motivation for this paper is the fact that the detection of

^{*} e-mail: sandri@ari.uni-heidelberg.de

BAOs as a modulation feature in the galaxy field depends on the assumption of a biasing mechanism (Gaztañaga et al. 2009; Desjacques et al. 2010) which relates the galaxy number density to the ambient density of dark matter as well as a control of redshift space distortions effects (Nishimichi et al. 2007; Taruya et al. 2009) and it would be desirable to measure the dark matter density directly. Weak lensing would be a prime candidate for such a measurement, but the wide line-of-sight weighting functions cause the weak lensing signal to depend rather on the integral of the spectrum of cold dark matter (CDM) than on individual, localized features, even in the case of tomographic lensing surveys (Hu 1999). This is the reason why investigate the sensitivity of 3d weak lensing (3dWL, Heavens 2003) for constraining the dark matter spectrum on BAO scales: 3dWL provides a direct estimate of the 3-dimensional matter distribution and gives Gaussian errors on the amplitude of the CDM spectrum in wavelength bands from sparsely sampled data (Leonard et al. 2012). In this way, we aim to quantify the statistical precision at which 3dWL constraints the CDM spectrum at the BAO wavelengths, and the statistical significance for inferring the presence of one or more wiggles from 3dWL data relative to the null-hypothesis of absent wiggles.

After a short compilation of basic results concerning distances, structure growth, structure statistics, and conventional weak lensing in Sect. 2, we recapitulate the main results of 3dWL in Sect. 3 and motivate its usage in constraining BAO wiggles. Our statistical approach and the estimation of statistical errors on the BAO measurement is given in Sect. 4, followed by a discussion of our main results in Sect. 5.

The reference cosmological model used is a spatially flat w CDM cosmology with Gaussian adiabatic initial perturbations in the matter distribution. The specific parameter choices are $\Omega_m = 0.25$, $n_s = 1$, $\sigma_8 = 0.8$ and $H_0 = 100 h$ km/s/Mpc, with $h = 0.72$. The dark energy equation of state is set to $w = -0.9$ and we assume the dark energy to be smooth. The baryon density $\Omega_b = 0.04$ is used for correcting the CDM shape parameter and for predicting BAO-wiggle amplitudes and wave-vectors.

2 COSMOLOGY AND STRUCTURE FORMATION

2.1 Dark energy cosmologies

In spatially flat dark energy cosmologies with the present matter density Ω_m , the Hubble function $aH(a) = da/dt$ is given by

$$\frac{H^2(a)}{H_0^2} = \frac{\Omega_m}{a^3} + (1 - \Omega_m) \exp\left(3 \int_a^1 d \ln a (1 + w(a))\right), \quad (1)$$

with the dark energy equation of state $w(a)$. A constant value $w \equiv -1$ corresponds to the cosmological constant. The relation between comoving distance χ and scale factor a is given by

$$\chi = c \int_a^1 \frac{da}{a^2 H(a)}, \quad (2)$$

with the Hubble distance $\chi_H = c/H_0$ as the cosmological distance scale. Redshift z and comoving distance are related by $dz/d\chi = H(z)/c$.

2.2 CDM power spectrum

The linear CDM-density power spectrum $P(k)$ describes the fluctuation amplitude of the Gaussian homogeneous density field δ ,

$$\langle \delta(\mathbf{k}) \delta(\mathbf{k}')^* \rangle = (2\pi)^3 \delta_D(\mathbf{k} - \mathbf{k}') P(k) \propto k^{n_s} T^2(k), \quad (3)$$

with the spectral index n_s and the transfer function $T(k)$. The restoring force provided by the baryon-photon fluid in the early Universe generates a set of wiggles in the spectrum $P(k)$ and an overall suppression due to diffusion. Both effects are discussed in detail by Eisenstein & Hu (1998) and Eisenstein & Hu (1999) who also provide a fitting formula for $T(k)$ in terms of the density parameters Ω_m , Ω_b , and the Hubble parameter h .

The spectrum $P(k)$ is normalized in such a way that it exhibits the variance σ_8^2 on the scale $R = 8$ Mpc/ h ,

$$\sigma_R^2 = \int \frac{k^2 dk}{2\pi^2} P(k) W^2(kR) \quad (4)$$

with a Fourier transformed spherical top hat filter function, $W(x) = 3j_1(x)/x$, where $j_\ell(x)$ is the spherical Bessel function of the first kind of order ℓ (Abramowitz & Stegun 1972).

2.3 Structure growth

The growth of density fluctuations in the cosmic matter distribution can be described as a self-gravitating hydrodynamical phenomenon, in the limit of Newtonian gravity. Homogeneous growth of the density field

$$\delta(\mathbf{x}, a) = D_+(a) \delta(\mathbf{x}, a = 1) \quad (5)$$

in the linear regime $|\delta| \ll 1$ is described by the growth function $D_+(a)$, which is the solution to the growth equation (Turner & White 1997; Wang & Steinhardt 1998; Linder & Jenkins 2003),

$$\frac{d^2}{da^2} D_+(a) + \frac{1}{a} \left(3 + \frac{d \ln H}{d \ln a} \right) \frac{d}{da} D_+(a) = \frac{3}{2a^2} \Omega_m(a) D_+(a). \quad (6)$$

Nonlinear structure formation leads to a strongly enhanced structure growth on small scales, generates non-Gaussian features and, most importantly, wipes out BAO wiggles as features in the initial matter distribution. This can be understood in an intuitive way as corrections to the CDM spectrum in perturbation theory to order n assume the shape of integrals over polyspectra up to order $2n$ (which separate into a product of n spectra by application of the Wick's theorem, see the review by Bernardeau et al. 2002) and are therefore becoming insensitive to localized features that are not strongly influencing the normalization of $P(k)$ (Springel et al. 2005; Jeong & Komatsu 2006; Pietroni 2008; Matarrese & Pietroni 2008; Crocce & Scoccimarro 2008; Nishimichi et al. 2009; Jeong & Komatsu 2009; Jürgens & Bartelmann 2012; Anselmi & Pietroni 2012). Since nonlinear structure formation affects small scales first, we will target BAO wiggles with 3dWL beginning at the largest wavelength before proceeding to successively shorter wavelengths.

2.4 Weak gravitational lensing

The weak lensing convergence κ provides a weighted line-of-sight average of the matter density δ (for reviews, see Bartelmann & Schneider 2001; Munshi et al. 2008; Hoekstra & Jain 2008; Bartelmann 2010),

$$\kappa = \int_0^{\chi_H} d\chi W_\kappa(\chi) \delta, \quad (7)$$

with the weak lensing efficiency $W_\kappa(\chi)$ as the weighting function,

$$W_\kappa(\chi) = \frac{3\Omega_m}{2\chi_H^2} \frac{D_+}{a} G(\chi) \chi, \quad (8)$$

and the lensing efficiency weighted galaxy redshift distribution, rewritten in terms of comoving distance,

$$G(\chi) = \int_{\chi}^{\chi_H} d\chi' n(\chi') \left(1 - \frac{\chi'}{\chi}\right). \quad (9)$$

$n(z)$ denotes a common parametrization of the redshift distribution of the lensed background galaxy sample,

$$n(z) = n_0 \left(\frac{z}{z_0}\right)^2 \exp\left(-\left(\frac{z}{z_0}\right)^\beta\right) dz \quad \text{with} \quad \frac{1}{n_0} = \frac{z_0}{\beta} \Gamma\left(\frac{3}{\beta}\right), \quad (10)$$

which can be rewritten in terms of a distribution in comoving distance with the relation $n(\chi)d\chi = n(z)dz$ using $d\chi/dz = c/H(a)$. These expressions allow to carry out a Limber projection (Limber 1954) of the weak lensing convergence, which yields the angular convergence spectrum $C_\kappa(\ell)$,

$$C_\kappa(\ell) = \int_0^{\chi_H} \frac{d\chi}{\chi^2} W_\kappa^2(\chi) P(k = \ell/\chi). \quad (11)$$

We will formulate our derivations in terms of the lensing convergence κ instead of the observable shear γ because it is a scalar quantity and possesses identical statistical properties. Eqn. (11) illustrates why line-of-sight averaged weak lensing spectra are ineffective in picking up BAO wiggles (and is almost a repetition of the previous argument why nonlinear structure formation destroys BAO features): They provide only an integrated measure of the CDM spectrum $P(k)$ weighted with wide weighting functions $W_\kappa(\chi)$ that is very insensitive to local features of the spectrum such as BAO wiggles. This argument holds even for advanced tomographic surveys (Hu 1999; Takada & Jain 2004) and motivates the need of a 3-dimensional mapping of the cosmic matter distribution. With reference to Gaztañaga et al. (2009) and Kazin et al. (2010), we would like to emphasize that weak lensing, due to its sensitivity to gravitational shear components perpendicular to the line of sight, will provide measurements of BAO wiggles in the transverse direction.

3 3D WEAK LENSING

The method of 3dWL was introduced by Heavens (2003), who proposed to include distances of lensed galaxies estimated from their photometric redshifts to infer the 3-dimensional *unprojected* tidal shear, i.e. the second derivatives of the gravitational potential perpendicular to the line-of-sight from distortions in the galaxies' ellipticity. Therefore, this approach differs from estimations of the angular line-of-sight averaged spectrum $C_\kappa(\ell)$ or corresponding tomographic spectra $C_\kappa^{ij}(\ell)$ in the important respect that the statistics of the full 3-dimensional matter distribution is inferred without any averaging of shears with the line-of-sight galaxy distribution, which has been performed in eqn. (9). As such, 3dWL is particularly suited for the problem at hand, namely to provide a precise estimate of the amplitude of the dark matter power spectrum at the BAO wavelengths. Additionally, Heavens (2003) showed that if 3dWL is used for constraining $P(k)$ at a fixed cosmology, the smallest errors are expected in the BAO regime of the CDM spectrum.

In this section, we recapitulate the main results of 3dWL in terms of the weak lensing convergence in the Fourier-convention we prefer to work with; please also refer to Castro et al. (2005), Massey et al. (2007), Heavens et al. (2006), Kitching et al. (2008) for a detailed description of the theory, to Munshi et al. (2011) for higher-order statistics through 3dWL and to Ayaita et al. (2012) for details of our numerical implementation. We assume spatial flatness and lensing in linearly evolving structures, which can be, in

principle, relaxed from the 3dWL point of view (Pratten & Munshi 2013). The impact of systematic errors is nicely investigated by Kitching et al. (2008), and for an application to observational data we refer the reader to Kitching et al. (2007).

The most natural choice for carrying out a Fourier transform in spherical coordinates is a combination of spherical harmonics for the angular and spherical Bessel functions for the radial dependence. We can therefore write the transformation for the convergence κ as

$$\kappa_{\ell m}(k) \equiv \sqrt{\frac{2}{\pi}} \int \chi^2 d\chi d\Omega \kappa(\chi, \theta) j_\ell(k\chi) Y_{\ell m}^*(\theta), \quad (12)$$

(see Ballinger et al. 1995; Heavens & Taylor 1995), where j_ℓ and $Y_{\ell m}$ are, respectively, a spherical Bessel function of the first kind and a spherical harmonic, and $\theta \equiv (\theta, \varphi)$. There exist algorithms for fast computation of $\kappa_{\ell m}(k)$ (Percival et al. 2004; Rassat & Refregier 2012; Lanusse et al. 2012; Leistedt et al. 2012). Such a transformation is particularly convenient as the combination of j_ℓ and $Y_{\ell m}$ is an eigenfunction of the Laplacian in spherical coordinates, leading to a quite simple relationship between the coefficients of the density field $\delta_{\ell m}(k)$ and the lensing convergence $\kappa_{\ell m}(k)$ as the observable:

$$\kappa_{\ell m}(k) = \frac{3\Omega_m}{2\chi_H^2} \frac{\ell(\ell+1)}{2} \frac{\eta_\ell(k, k')}{(k')^2} \delta_{\ell m}(k'), \quad (13)$$

with the lensing-induced mode coupling $\eta_\ell(k, k')$

$$\eta_\ell(k, k') = \frac{4}{\pi} \int_0^\infty \chi'^2 d\chi' \int_0^{\chi'} d\chi \frac{\chi' - \chi}{\chi\chi'} \frac{D_+}{a} j_\ell(k\chi') j_\ell(k'\chi), \quad (14)$$

with implicit assumption of the Einstein summation convention

$$X(k, k') Y(k', k'') \equiv \int_0^\infty k'^2 dk' X(k, k') Y(k', k''). \quad (15)$$

It is then possible to construct an estimator for $\kappa_{\ell m}(k)$ by including the uncertainty of the galaxy distance estimates coming from errors in the measurements of redshift. If we denote by χ the true radial coordinate of a galaxy, and by χ' the one inferred by its observed redshift $z' = z(\chi')$, then they will be related by the probability $p(\chi'|\chi)$, which we assume to be Gaussian for simplicity:

$$p(\chi'|\chi) d\chi = \frac{1}{\sqrt{2\pi\sigma_z^2}} \exp\left[-\frac{(z(\chi) - z(\chi'))^2}{2\sigma_z^2}\right] dz', \quad (16)$$

where σ_z is the width of the distribution and is assumed to be constant throughout the entire galaxy sample. Furthermore, galaxies receive a statistical weight according to their distribution in distance $n(\chi)d\chi$. Following the derivation in Heavens (2003), we define the two additional matrices

$$Z_\ell(k, k') = \frac{2}{\pi} \int \chi'^2 d\chi' \int d\chi p(\chi'|\chi) j_\ell(k'\chi) j_\ell(k\chi'), \quad (17)$$

$$M_\ell(k, k') = \frac{2}{\pi} \int \chi^2 d\chi n(\chi) j_\ell(k\chi) j_\ell(k'\chi), \quad (18)$$

where $n(\chi)$ is the number density of galaxies, as defined in eqn. (10). These matrices describe the correlations in spherical Fourier modes generated by the measurement process: While $\eta_\ell(k, k')$ describes mode couplings due to weak lensing, $Z_\ell(k, k')$ and $M_\ell(k, k')$ define, respectively, the contributions in the mode couplings coming from redshift errors and from the galaxy distribution along the radial coordinate χ .

We restrict ourselves to observations of the entire sky. In this case, the expression for the estimator $\bar{\kappa}_{\ell m}$ of the convergence is then expected to be

$$\bar{\kappa}_{\ell m}(k) = \frac{3\Omega_m}{2\chi_H^2} \frac{\ell(\ell+1)}{2} \frac{B_\ell(k, k'')}{(k'')^2} \delta_{\ell m}(k''). \quad (19)$$

where the mode-coupling matrix $B_\ell(k, k')$ describes two integrations over k_1 and k_2 :

$$B_\ell(k, k'') = Z_\ell(k, k_1) M_\ell(k_1, k_2) \eta_\ell(k_2, k''). \quad (20)$$

Since the average values of a field like $\kappa_{\ell m}(k)$ are zero for all-sky surveys, we can only infer information about any parameter the field may depend on by means of its covariance,

$$\langle \bar{\kappa}_{\ell m}(k) \bar{\kappa}_{\ell m}^*(k') \rangle = S_{\kappa, \ell}(k, k') + N_{\kappa, \ell}(k, k') \equiv C_{\kappa, \ell}(k, k') \quad (21)$$

which consists of a signal term $S_{\kappa, \ell}(k, k')$ and a noise term $N_{\kappa, \ell}(k, k')$. The signal term $S_{\kappa, \ell}$ can be calculated directly from eqn. (19):

$$S_{\kappa, \ell}(k, k') = \left(\frac{3\Omega_m}{2\chi_H^2} \right)^2 \left[\frac{\ell(\ell+1)}{2} \right]^2 \frac{B_\ell(k, k'')}{(k'')^2} \frac{B_\ell(k', k'')}{(k'')^2} P_\delta(k''), \quad (22)$$

with the abbreviations

$$B_\ell(k, k'') = Z_\ell(k, k_1) M_\ell(k_1, k_2) \eta_\ell(k_2, k'') \quad (23)$$

$$B_\ell(k', k'') = Z_\ell(k', k_3) M_\ell(k_3, k_4) \eta_\ell(k_4, k'') \quad (24)$$

with implicit integration over k_1, k_2 and k_3, k_4 . The corresponding noise part $N_{\kappa, \ell}$ is given by

$$N_{\kappa, \ell}(k, k') = \frac{\sigma_\epsilon^2}{4} M_\ell(k, k'), \quad (25)$$

which is proportional to the shape noise σ_ϵ^2 , namely the variance of the galaxy ellipticity distribution. It is important to notice that $N_{\kappa, \ell}$ is independent of cosmology or variations in the CDM spectrum $P(k)$. Intrinsic ellipticity correlations were neglected, which would greatly complicate the 3dWL description.

4 DETECTING BAO WIGGLES

4.1 Construction of the Fisher matrix

We choose a Fisher matrix approach to determine how precisely 3dWL can constrain baryon acoustic oscillations in the matter power spectrum $P(k)$. The Fisher matrix is a square matrix whose elements are defined as the expectation values of the second derivative of the logarithmic likelihood with respect to the fiducial parameters θ_α and θ_β :

$$F_{\alpha\beta} = - \left\langle \frac{\partial^2 \ln \mathcal{L}}{\partial \theta_\alpha \partial \theta_\beta} \right\rangle. \quad (26)$$

As a general statement, if the likelihood \mathcal{L} can be expressed as an N -dimensional Gaussian

$$\mathcal{L} = \frac{1}{\sqrt{(2\pi)^N \det(C)}} \exp \left(-\frac{1}{2} \vec{x}^T C^{-1} \vec{x} \right), \quad (27)$$

where \vec{x} is a generic data vector and C is the corresponding covariance, we can then write

$$F_{\alpha\beta} = \frac{1}{2} \text{tr} \left[(C^{-1} \partial_\alpha C) \times (C^{-1} \partial_\beta C) \right], \quad (28)$$

or, equivalently,

$$F_{\alpha\beta} = \frac{1}{2} \text{tr} \left[\partial_\alpha \ln C \times \partial_\beta \ln C \right], \quad (29)$$

where ∂_α and ∂_β stand for the derivatives with respect to the parameters θ_α and θ_β . Given a particular experimental framework, the

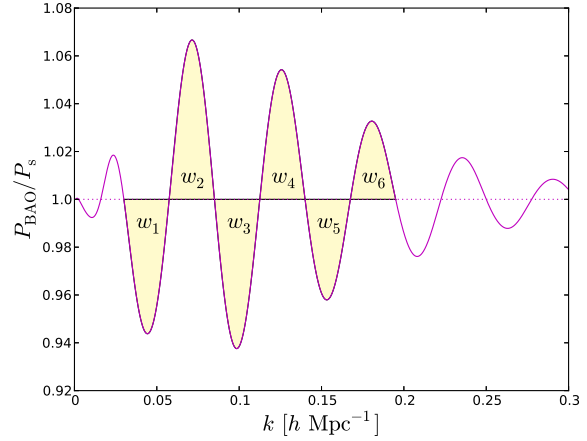


Figure 1. Ratio between the power spectrum with baryon acoustic oscillations $P(k)$ and the smooth power spectrum $P_s(k)$. The largest wiggles in amplitude have been highlighted and labeled as $w_\alpha, \alpha = 1, \dots, 6$. These are the wiggles used to parametrize the power spectrum in our Fisher matrix approach.

Fisher matrix specifies what are the best errors to expect for the inferred parameters θ_α via the Cramér-Rao relation.

It can be proved that, since ℓ -measurements are independent in the case of full-sky coverage, we can reformulate eqn. (28): we consider our estimator to be $\bar{\kappa}_{\ell m}(k)$ and its covariance as defined in eqn. (21), and find

$$F_{\alpha\beta} = \frac{f_{\text{sky}}}{2} \sum_{\ell=\ell_{\min}}^{\ell_{\max}} (2\ell+1) \text{tr} \left[(C_{\kappa, \ell}^{-1} \partial_\alpha C_{\kappa, \ell}) \times (C_{\kappa, \ell}^{-1} \partial_\beta C_{\kappa, \ell}) \right]. \quad (30)$$

In our specific case, we consider the power spectrum as parametrized not by usual cosmological parameters, such as Ω_m or σ_8 , but rather by its own wiggles amplitudes, namely by the values assumed by $P(k)$ in a range of k where the wiggles w_α are located. In Fig. 1 we plot the wiggle-only power spectrum, i.e. the ratio between the power spectrum with baryon acoustic oscillations $P(k)$ and an equivalent, smoothed out spectrum that has the same shape as $P(k)$ but shows no oscillating feature, $P_s(k)$. We highlight the wiggles that have been used to parametrize $P(k)$, $w_\alpha, \alpha = 1, \dots, 6$. By calculating the derivative $\partial_\alpha C$ of the covariance with respect to a variation of the amplitude of a maximum number of wiggles n_w , we can build up (eqn. 28) a Fisher matrix $F_{\alpha\beta}$, where $\alpha, \beta = 1, \dots, n_w$. Such a matrix carries information about the best errors to expect on the detection of each wiggle $w_\alpha, \alpha = 1, \dots, n_w$, and the cross-correlations between inferred wiggle amplitudes. Given our aim, what we are actually performing in the calculation of $\partial_\alpha C$ is a functional derivative, also known as Fréchet derivative. In fact, we can imagine the power spectrum as depending on features, i.e. the wiggles in Fig. 1. Each one of them can be approximated to a sin-like function defined in a range of k as wide as $\lambda/2$, where λ is the wavelength of the function itself. The covariance derivative is numerically estimated for one wiggle at a time as a finite difference:

$$\partial_\alpha C_{\kappa, \ell} = \frac{C_{\kappa, \ell, \alpha}^+ - C_{\kappa, \ell, \alpha}^-}{2\epsilon}, \quad (31)$$

where $C_{\kappa, \ell, \alpha}^\pm$ are the covariance matrices calculated using the power spectra $P_\alpha^\pm(k)$ and ϵ is an arbitrarily small number. The spectra $P_\alpha^\pm(k)$ are equivalent to the original $P(k)$ for all k of the domain,

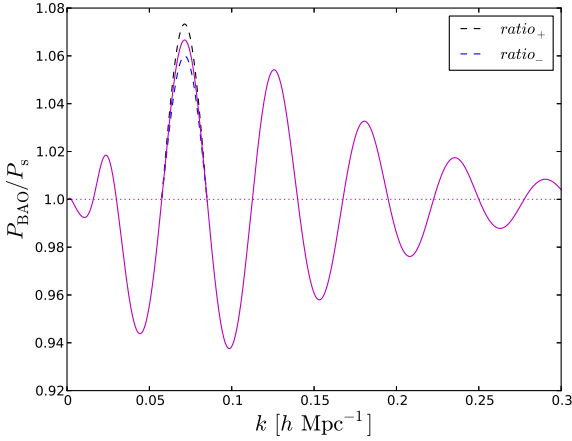


Figure 2. The ratio between $P(k)$ and $P_s(k)$. The figure shows a pictorial representation of the variation of the amplitude of one wiggle when calculating the derivative of the covariance matrix, $\partial_{\alpha=2}C_\ell$.

	z_{med}	\bar{n}	f_{sky}	σ_z	σ_ϵ
EUCLID	0.9	30	0.5	0.1	0.3
DES	0.7	10	0.1	0.02	0.3
DEEP	1.5	40	0.1	0.05	0.3

Table 1. Basic survey characteristics used for the Fisher-analysis: median redshift z_{med} of the galaxy sample, galaxy density per squared arcminute \bar{n} , sky coverage fraction f_{sky} , redshift error σ_z and shape measurement error σ_ϵ of the surveys EUCLID, DES and a hypothetical deep-reaching survey labeled DEEP.

exception made for the wave numbers belonging to the interval I_α that corresponds to wiggle w_α . In this interval $P_\alpha^\pm(k)$ is then

$$P_\alpha^\pm(k) = P(k) \pm \epsilon P(k). \quad (32)$$

We would like to point out that, since what we are actually performing by means of the spectrum variation in eqn. (32) is in a way a logarithmic derivative of C_ℓ , the denominator in eqn. (31) lacks a factor $P(k)$ and is therefore just two times the fraction of the spectrum used in the variation. In Fig. 2 we show a representation of an example of the variation performed in the calculation of the derivative of the covariance matrix, $\partial_\alpha C$; in this case the second wiggle, w_2 , has been considered.

It is worth noticing that the Fisher-matrix approach for inferring the error σ_α on the dark matter spectrum $P(k_\alpha)$ (where k_α are simply the $k \in I_\alpha$, for brevity) as a Gaussian standard deviation is perfectly justified because of the linearity of the lensing observable and the linearity of the random field, so we do not need to use Monte-Carlo sampling for evaluating the likelihood $\mathcal{L}(P(k_\alpha))$ and to measure its widths σ_α from Monte-Carlo samples of the likelihood.

As noise sources for the inference of $P(k_\alpha)$, we consider a Gaussian shape measurement error σ_ϵ for the galaxy ellipticities, which are assumed to be intrinsically uncorrelated, and a Gaussian error σ_z for the redshift determination uncertainty. Likewise, we work in the approximation of neglecting all geodesic effects (Seitz & Schneider 1994; Seitz et al. 1994) like deviations from the Born approximation, lens-lens couplings (Shapiro & Cooray 2006; Krause & Hirata 2010), source clustering (Schneider et al. 2002),

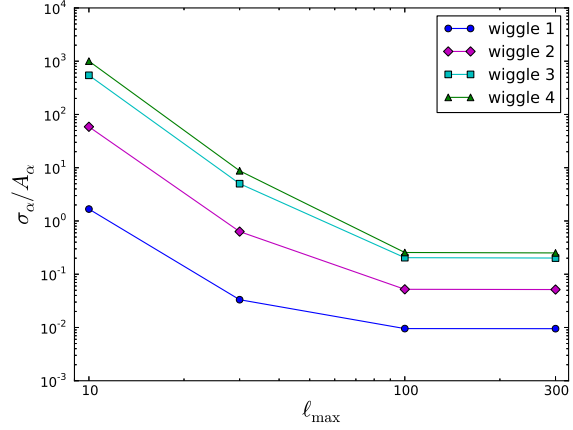


Figure 3. The marginalized errors on the first four wiggles, normalized with respect to their amplitude, as the maximum ℓ used for the calculation of the Fisher matrix increases. It shows that choosing $\ell_{\text{max}} > 100$ brings no particular advantage in the precision of the wiggles measurement. In the calculation of the errors we considered the power spectrum as parametrized by the first 4 wiggles.

source-lens correlations (Hamana et al. 2002), and deviations from Newtonian gravity (Acquaviva et al. 2004). While performing the necessary variations for computing the Fisher matrix, we keep all other cosmological parameters fixed and calculate everything using an ℓ -range between $\ell_{\text{min}} = 2$ and $\ell_{\text{max}} = 100$ (please see the next section for a justification of this choice). As surveys, we consider the cases of EUCLID, DES, and a hypothetical deep-reaching galaxy survey we refer to by the name DEEP. The respective survey properties are summarized in Table 1. All the details concerning the numerical implementation used in the calculation of the covariance matrices can be found in Ayaita et al. (2012).

4.2 Statistical errors

The error σ_α for inferring the amplitude of the CDM spectrum $P(k_\alpha)$ at wiggle positions k_α is given by the Cramér-Rao relation,

$$\sigma_\alpha^2 = (F^{-1})_{\alpha\alpha}, \quad (33)$$

and

$$\sigma_\alpha^2 = 1/F_{\alpha\alpha}, \quad (34)$$

for marginalized and conditional likelihoods, respectively.

Before carrying out our analysis for surveys like EUCLID, DES, and DEEP, we implement some tests in order to determine the optimal value for the maximum number of modes to be used in the calculation of the Fisher matrix, ℓ_{max} . Besides, we tried to find out how and by how much are the errors sensitive to some of the usual survey parameters, such as

- (i) the shape noise σ_ϵ ;
- (ii) the error σ_z in the measurement of redshift;
- (iii) the median redshift z_{med} ;
- (iv) the fraction of sky coverage f_{sky} .

Throughout these tests, when not stated otherwise, we make use of a default set of survey parameters such that $\sigma_z = 0.02$, $\sigma_\epsilon = 0.3$, $z_{\text{med}} = 0.9$, $f_{\text{sky}} = 0.4$ and $\bar{n} = 20$. Additionally, we assumed we want to constrain simultaneously the first four wiggles (see Fig. 1).

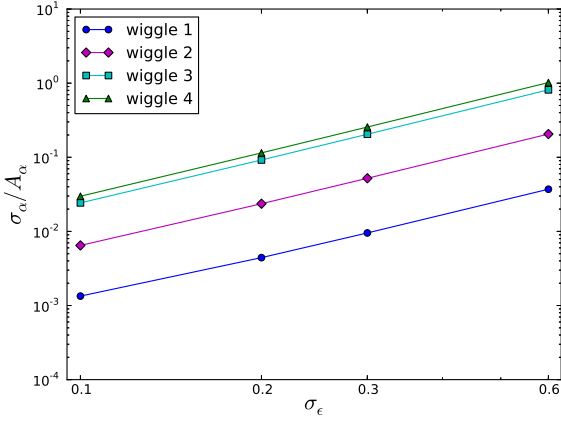


Figure 4. The relative marginalized error for the first 4 wiggles, as the shape noise σ_ϵ varies. Again, we assumed $\sigma_z = 0.02$, $\sigma_\epsilon = 0.3$, $z_{\text{med}} = 0.9$, $f_{\text{sky}} = 0.4$ and $\bar{n} = 20$. As we expected, larger values of σ_ϵ bring along larger errors on the detection of the wiggles.

We start our investigation by determining the errors σ_α , $\alpha = 1, 2, 3, 4$, as the maximum number of modes ℓ_{max} in the summation in eqn. (30) increases. Please refer to Fig. 3 for a plot of the behavior of σ_α normalized to the oscillation amplitude A_α , where A_α is defined as the maximum value of $|P(k) - P_s(k)|$ for each wiggle. In particular, we considered $\ell_{\text{max}} = 10, 30, 100, 300$, and observe that, after $\ell_{\text{max}} = 100$, there is practically no gain in the precision with which the first 4 wiggles would be constrained in a 3dWL approach. Therefore, we decide to stick to a maximum number of modes of 100 for all the subsequent calculations. This is a fair approximation also from a theoretical point of view: in fact, extending too much the ℓ interval for the $F_{\alpha\beta}$ summation could make us fall out of the linear regime; in addition, the assumption of a Gaussian shape for the likelihood \mathcal{L} could not be anymore reasonable in such a multipole range (Heavens 2003).

In Fig. 4, we show what happens as soon as we keep all the survey parameters fixed and vary the shape noise σ_ϵ . As one can expect, larger values of σ_ϵ lead to larger σ_α , therefore to a greater uncertainty in the detection of the wiggles. Moreover, the rate at which σ_α grows with the shape noise seems to be of the type of a power law, and seems independent of the wiggle considered, at least for the wiggles sample we evaluated. The situation turns out to be similar when the error in the determination of redshift σ_z is considered, in Fig. 5: increasing σ_z still produces larger errors on all the wiggles under investigation, although here the relation is somewhat slower, especially as long as $\sigma_z \lesssim 0.1$; the relation also appears to be slightly dependent on the wiggle, becoming steeper as higher order oscillations are taken. In fact, by incrementing the error on redshift from 0.01 to 0.1, we get an error larger only by a factor of ~ 2 on the first wiggle and by a factor of ~ 8 on the second. Additionally, the correspondence between σ_α and the median redshift of the survey (Fig. 6) seems again like a power law that gives larger errors for an increasing z_{med} , and is independent of the wiggle. Qualitatively, this trend makes sense in light of the fact that, as we increase the median redshift, we keep fixed all other survey parameters such as, for example, the galaxy density per squared arcminute \bar{n} . By doing so, we consider surveys where a number \bar{n} of galaxies is distributed over a deeper cone, meaning that we are actually sampling the 3D convergence field in a more diluted way,

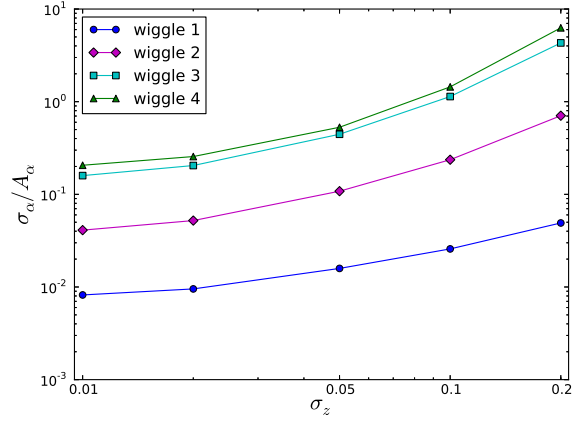


Figure 5. The relative marginalized error for the first 4 wiggles as a function of the error in the measurement of the photometric redshift, σ_z . The sensitivity of the errors on the value of σ_z is not as steep as it is for the shape noise σ_ϵ . In addition, the increasing rate of σ_α seems to change as we consider higher order wiggles.

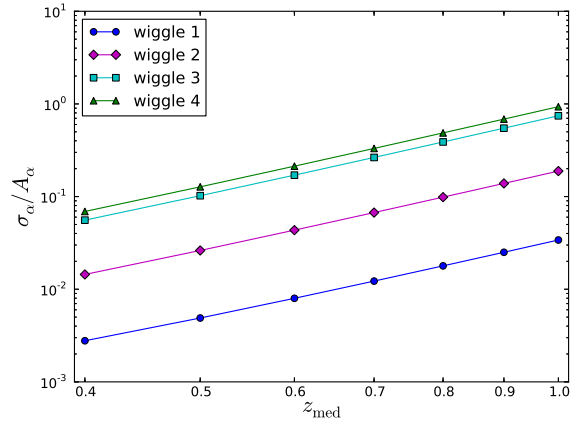


Figure 6. Relative marginalized errors on the first 4 wiggles when the median redshift z_{med} of the survey increases. Since all other parameters are kept fixed, especially the mean galaxy density per squared arcminute, \bar{n} , increasing z_{med} is equivalent to having more and more diluted surveys, where the same amount of galaxies is distributed along a deeper survey cone.

and therefore inheriting a larger noise. Naturally, varying the sky coverage propagates to the errors $\sigma_\alpha \propto 1/\sqrt{f_{\text{sky}}}$.

4.3 Detectability of BAO wiggles

In this section, we would like to present the results obtained when estimating the best errors to expect on BAO wiggles for the surveys EUCLID, DES, and DEEP (please see Table 1 for specifications).

We started our analysis by calculating both marginalized ($\sigma_\alpha = \sqrt{(F^{-1})_{\alpha\alpha}}$) and conditional errors ($\sigma_\alpha = 1/\sqrt{F_{\alpha\alpha}}$) relative to the wiggle amplitude. These errors were computed for the three types of surveys, considering the first four oscillations, as shown in Fig. 7. As we could expect, marginalized errors are always larger than the correspondent conditional ones, namely the σ_α on each

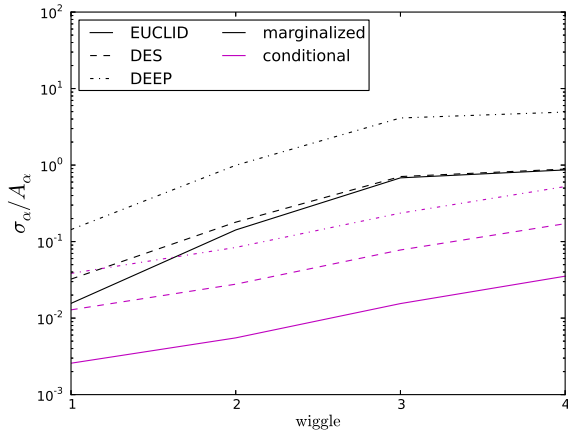


Figure 7. Conditional (magenta lines) and marginalized relative errors (black lines) for the three surveys under investigations EUCLID (solid line), DES (dashed line) and DEEP (dash-dot line) as a function of the wiggles, when the first 4 oscillations are simultaneously constrained.

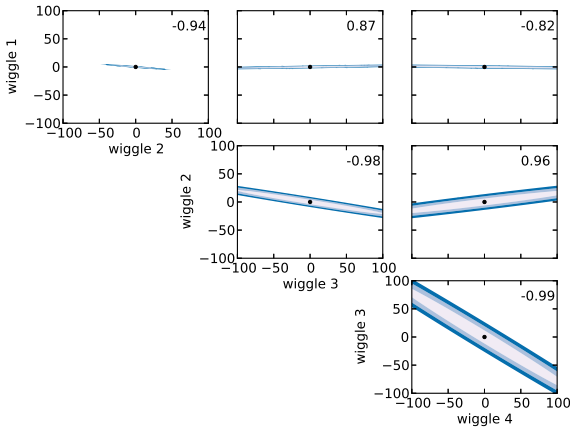


Figure 8. Confidence ellipses for the first four wiggles in a EUCLID-like survey, showing that the wiggles are indeed highly correlated. In fact, taking, for example, two consecutive wiggles, such as w_2 and w_3 , we see that by increasing the amplitude of $P(k)$ at the position of wiggle 2, we must then have the amplitude at w_3 decreased in order to remain in the confidence region. The x - and y -axes show the variation of the wiggle in terms of percentage of its amplitude A_α , the three contours areas correspond to $1 - 2 - 3\sigma$, and every panel shows the correlation coefficient in the upper-right corner.

wiggle when we assume to know precisely all the other wiggle amplitudes.

We continue the investigation considering the confidence ellipses calculated from the corresponding Fisher matrices obtained for the three surveys. We assume we are aiming to jointly constrain the first four wiggles and plot the results in Figs. 8, 9, and 10 for, respectively, EUCLID, DES, and DEEP. The sizes of the ellipses, whose contours stand for $1 - 2 - 3\sigma$, already tell us that, among the ones evaluated, EUCLID will probably be the survey with largest constraining power on the BAO wiggles. It is of particular interest noticing the orientation of the ellipses, or their correlation coefficients (upper-right corner in every panel), that tell us something

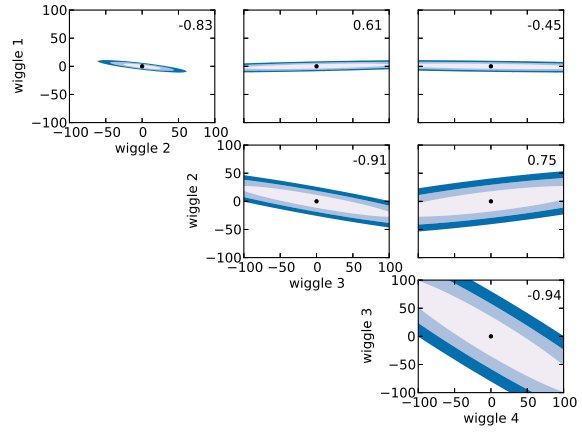


Figure 9. Fisher confidence ellipses for DES, when one tries to simultaneously constrain the first four wiggles. Again, contours areas correspond to $1 - 2 - 3\sigma$ and the number in every panel is the correlation coefficient; the axes represent variation of wiggles in terms of their amplitude fraction. Also in this case we can observe correlation between the amplitudes of $P(k)$ at different wiggles positions.

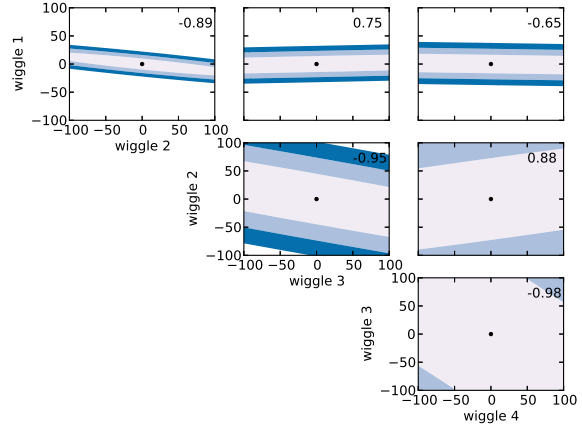


Figure 10. Confidence ellipses for the DEEP survey, with the variation of the oscillations in terms of the wiggle amplitude. Again, we assumed we wanted to constrain jointly the first four wiggles, contour areas stand for $1 - 2 - 3\sigma$ and the correlation coefficient can be read in the panels.

about the interdependence between different wiggles: in fact, neighboring wiggles are anti-correlated, i.e. increasing the amplitude of the power spectrum in correspondence to one oscillation would cause the $P(k)$ at the position of the adjacent wiggle to take smaller values in order to stay among the confidence region, and vice versa, whereas the opposite holds for alternated wiggles.

In order to better understand whether the constraining power of the three surveys will allow us to detect any oscillatory feature in the CDM power spectrum, we plot the σ_α obtained from the Cramér-Rao relation in eqn. (33) as error bars in the usual wiggle-only power spectrum for DEEP (Fig. 13), DES (Fig. 12), and EUCLID (Fig. 11). Since what is shown is a ratio between $P(k)$ and a smooth spectrum, the σ_α have of course also been normalized with respect to $P_s(k)$. The four different panels show how the errors

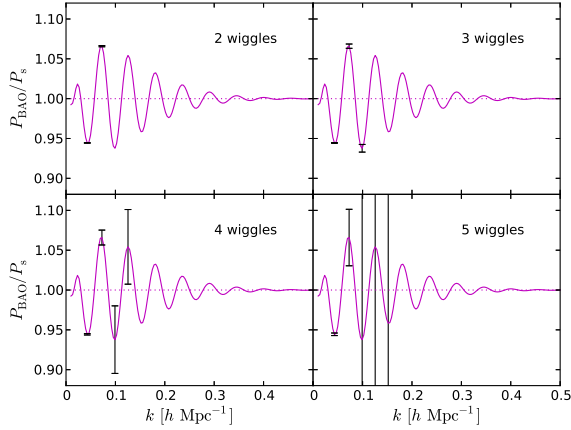


Figure 11. The bars show the marginalized errors in the detection of the wiggles, normalized with respect to $P_s(k)$, when the first 2 (upper left panel), 3 (upper right panel), 4 (bottom left panel), 5 (bottom right panel) wiggles are used to parametrize the power spectrum. Here, we considered a EUCLID-like survey with $\sigma_z = 0.1$, $\sigma_\epsilon = 0.3$, $z_{\text{med}} = 0.9$, $f_{\text{sky}} = 0.5$ and $\bar{n} = 30$.

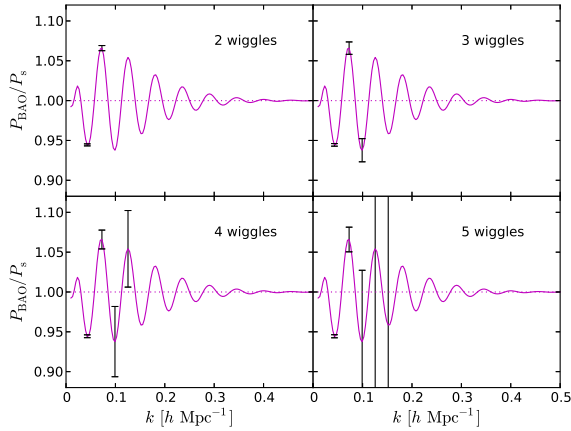


Figure 12. Marginalized errors on the detection of BAO wiggles when one tries to detect the first 2 (upper left panel), 3 (upper right panel), 4 (bottom left panel), 5 (bottom right panel) wiggles at the same time, for a DES-like survey ($\sigma_z = 0.02$, $\sigma_\epsilon = 0.3$, $z_{\text{med}} = 1.5$, $f_{\text{sky}} = 0.12$ and $\bar{n} = 10$). Again, we considered the relative marginalized errors, dividing by $P_s(k)$.

change when we try to jointly constrain the first 2, 3, 4, or 5 wiggles with a 3dWL approach.

What these and the following plots show, first of all, is an expected feature: as we increment the number of wiggles we expect to simultaneously examine, the precision with which the amplitudes $P(k_\alpha)$ would be measured gets poorer and poorer for all the oscillations. Our purpose would then be to evaluate how many BAO wiggles one is allowed to constrain before the errors on them become too large. It can be seen that all three surveys would allow for quite good constraints on the first 2 wiggles. The hypothetical survey DEEP already shows error bars of the order of the wiggle amplitude A_α when the first 3 wiggles are considered, and the errors become much larger than A_α ($\alpha > 1$) as soon as one tries to detect 4 or more wiggles (Fig. 13). On the other hand, DES and

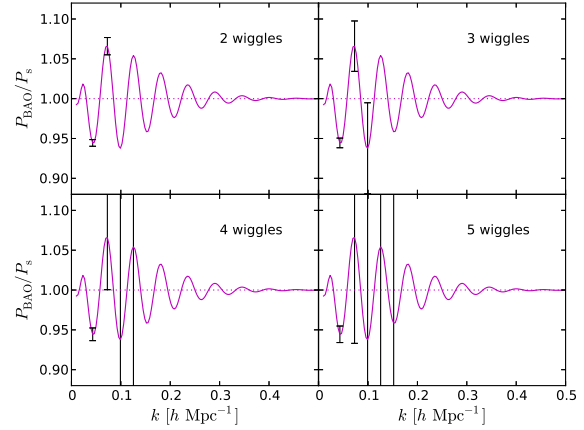


Figure 13. The marginalized errors on the detection of the wiggles in the power spectrum, relative to $P_s(k)$, for the hypothetical survey DEEP, characterized by the parameters $\sigma_z = 0.02$, $\sigma_\epsilon = 0.3$, $z_{\text{med}} = 1.5$, $f_{\text{sky}} = 0.1$ and $\bar{n} = 40$.

EUCLID give a better performance, allowing for up to 4 wiggles to be simultaneously constrained, with EUCLID giving smaller errors overall (Fig. 11).

A better comparison between the three surveys can be carried out analyzing Figs. 15 and 14, where we plotted relative errors σ_α/A_α as functions of the maximum number of wiggles we want to jointly constrain, n_w , and we collate results coming from, respectively, DEEP and EUCLID, and DES, and EUCLID. It becomes straightforward that a DEEP-like survey cannot compete against EUCLID: the relative errors coming from DEEP are always larger than the latter's, independently of the maximum number of wiggles to be constrained, and remain safely under the unity only for the first 2 wiggles.

The situation is better for DES, which gives results quite similar to EUCLID's up to $n_w = 4$, and an even higher performance afterwards, since its σ_α are increasing at a smaller pace with respect to EUCLID's. This is not very useful, anyway, as the relative errors become larger than 1 for $n_w > 4$ for both surveys.

Concluding, EUCLID seems to grant the best results, allowing for the simultaneous detection of up to 4 wiggles with expected errors that are smaller than the ones predicted for both DES and, of course, DEEP.

5 SUMMARY AND CONCLUSIONS

Subject of this paper has been a statistical investigation on whether future weak lensing surveys are able to detect baryon acoustic oscillations in the cosmic matter distribution by application of the 3d weak lensing method. For a fixed Λ CDM cosmology, we have estimated the statistical precision σ_α on the amplitude of the CDM spectrum $P(k)$ at the BAO wiggle positions in a Fisher-matrix approach. Throughout, we worked under the assumption of Gaussian statistics, independent Fourier modes and in the limit of weak lensing. Noise sources were idealized and consisted in independent Gaussian-distributed shape-noise measurements for the lensed background galaxy sample, as well as a Gaussian error for the redshift determination. As surveys, we considered the cases of EUCLID, DES and a hypothetical deep-reaching survey DEEP.

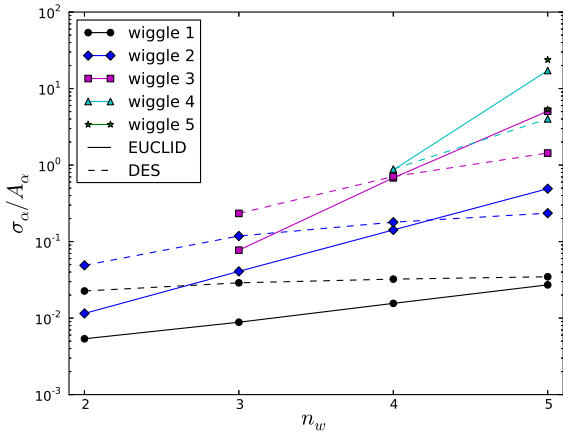


Figure 14. Relative marginalized errors (with respect to the wiggles amplitude) as a function of the maximum number of wiggles that we try to simultaneously detect, n_w . Here, we show the results for a EUCLID-like survey (solid lines) and a DES-like survey (dashed lines). Different colors and point types correspond to the different wiggles on which the error σ_α is calculated. The relative errors coming from a DES-like survey turn out to be larger than EUCLID’s as long as we try to observe a maximum of four wiggles. DES gives a better performance for $n_w > 4$, but the σ_α on the measurement of the higher order wiggles prove to be too large with respect to their amplitude A_α , anyway.

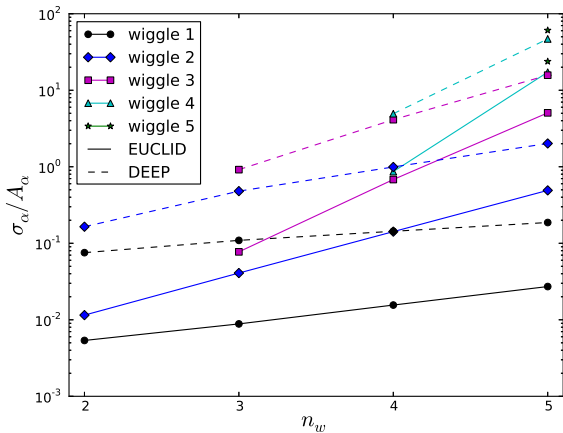


Figure 15. Relative marginalized errors as a function of n_w for a EUCLID-like survey (solid lines) and a DEEP-like survey (dashed lines). The relative σ_α for a DEEP survey appear to be always larger than the ones obtained from EUCLID, independently of the maximum number of wiggles n_w we want to constrain.

(i) We have constructed the Fisher matrix considering our model as parametrized by the amplitudes of the CDM power spectrum at the baryon acoustic oscillations anticipated positions. In particular, we started taking the two BAO wiggles with largest amplitude and progressively increased the number of oscillations considered. Keeping the cosmology fixed to a standard Λ CDM parameter choice, we carried out variations of $P(k)$ that preserved its wiggle-shape in those wave number intervals; we then estimated the Fisher matrix accordingly, in order to quantify whether the statistical power of future weak lensing surveys suffices to place bounds on the amplitudes of the considered harmonics. By means

of the Cramér-Rao relation, we calculated the best errors σ_α to expect for the amplitudes of $P(k)$ at wiggle positions.

(ii) The sensitivity of σ_α with respect to some typical survey-parameters was tested. In particular, we considered the shape noise σ_ϵ , the redshift error σ_z , the median redshift z_{med} , and the sky coverage f_{sky} . We found that, as expected, increasing the uncertainty in the estimate of either the redshift or the galaxy shapes brings a larger error in the inference of the presence of wiggles, and that the sensitivity of these errors on σ_z is less pronounced for small values of σ_z , although it grows as soon as we consider higher order wiggles or large σ_z . An increase of z_{med} leads as well to larger errors on the wiggles amplitudes, as one would expect from considering less and less populated surveys; for the same reason, a wider sky coverage, i.e. larger f_{sky} , yields to higher precision in constraining the wiggle amplitudes $\sigma_\alpha \propto 1/\sqrt{f_{\text{sky}}}$.

Overall, we may conclude that the volume of a survey seem to be overcoming the importance of a high precision in the redshift measurement of galaxies, at least for $\sigma_z < 0.1 - 0.2$.

(iii) Finally, we evaluated the σ_α for the surveys under investigation and found that, among them, EUCLID gave the best results, potentially allowing for the detection of up to the first four BAO wiggles with a good statistical confidence. Given our tests on the sensitivity of the errors on $P(k_\alpha)$ to certain survey parameters, we may conclude that EUCLID’s good performance is probably due to the volume of the survey in terms of total galaxy number and sky coverage, that seem to prevail over the negative effects brought by the error on redshift measurements, σ_z , quite larger than the ones predicted for the other two surveys.

Given these results, we conclude that measurements of BAO wiggles based on future weak lensing data are entirely possible, and avoid issues related to galaxy biasing and redshift-space distortions. We forecast a detection of the first four wiggles with EUCLID and DES by applying 3dWL techniques. Future developments from our side include estimates of the precision that can be reached on inferring dark energy density and equation of state by including the estimate of the BAO scale at low redshifts probed by lensing to the estimates at intermediate redshift provided by galaxy surveys and those at high redshifts such as the CMB. Additionally, we are investigating the impact of systematical errors on the estimation process from 3dWL-data and biases in the estimation of BAO-wiggle amplitudes.

ACKNOWLEDGEMENTS

Our work was supported by the German Research Foundation (DFG) within the framework of the excellence initiative through the Heidelberg Graduate School of Fundamental Physics. AG receives support from the Graduate School of Fundamental Physics (GSFP+), in addition AG would like to acknowledge support from the International Max-Planck Research School for Astronomy and Cosmic Physics. We would like to thank first of all Youness Ayaita and Maik Weber for the precious contribution to this work. We are also grateful to Matthias Bartelmann, Angelos Kalovidouris, Federica Capranico, and Philipp M. Merkel for their advice and suggestions, and of course to Alan Heavens, who was so kind to answer our questions at the Transregio Winter School in Passo del Tonale.

REFERENCES

Abramowitz M., Stegun I. A., 1972, Handbook of Mathemati-

- cal Functions. Handbook of Mathematical Functions, New York: Dover, 1972
- Acquaviva V., Baccigalupi C., Perrotta F., 2004, *Phys. Rev. D*, 70, 023515
- Angulo R. E., Baugh C. M., Frenk C. S., Lacey C. G., 2008, *MNRAS*, 383, 755
- Anselmi S., Pietroni M., 2012, *ArXiv e-prints* 1205.2235
- Ayaita Y., Schäfer B. M., Weber M., 2012, *MNRAS*, 422, 3056
- Ballinger W. E., Heavens A. F., Taylor A. N., 1995, *MNRAS*, 276, L59
- Bartelmann M., 2010, *Classical and Quantum Gravity*, 27, 233001
- Bartelmann M., Schneider P., 2001, *Physics Reports*, 340, 291
- Bassett B., Hlozek R., 2010, *Baryon acoustic oscillations*. p. 246
- Bennett C. L., Kogut A., Hinshaw G., Banday A. J., Wright E. L., Gorski K. M., Wilkinson D. T., Weiss R., et al., 1994, *ApJ*, 436, 423
- Bernardeau F., Colombi S., Gaztañaga E., Scoccimarro R., 2002, *Physics Reports*, 367, 1
- Beutler F., Blake C., Colless M., Jones D. H., Staveley-Smith L., Campbell L., Parker Q., Saunders W., Watson F., 2011, *MNRAS*, 416, 3017
- Busca N. G., Delubac T., Rich J., Bailey S., Font-Ribera A., Kirkby D., Le Goff J.-M., Pieri M. M., et al., 2012, *ArXiv e-prints* 1211.2616
- Cabré A., Gaztañaga E., 2011, *MNRAS*, 412, L98
- Castro P. G., Heavens A. F., Kitching T. D., 2005, *Phys. Rev. D*, 72, 023516
- Crocce M., Scoccimarro R., 2008, *Phys. Rev. D*, 77, 023533
- Desjacques V., Crocce M., Scoccimarro R., Sheth R. K., 2010, *Phys. Rev. D*, 82, 103529
- Dolney D., Jain B., Takada M., 2006, *MNRAS*, 366, 884
- Eisenstein D. J., Hu W., 1998, *ApJ*, 496, 605
- Eisenstein D. J., Hu W., 1999, *ApJ*, 511, 5
- Eisenstein D. J., Seo H.-J., Sirko E., Spergel D. N., 2007, *ApJ*, 664, 675
- Eisenstein D. J., Zehavi I., Hogg D. W., Scoccimarro R., Blanton M. R., Nichol R. C., Scranton R., Seo H.-J., et al., 2005, *ApJ*, 633, 560
- Gaztañaga E., Cabré A., Castander F., Crocce M., Fosalba P., 2009, *MNRAS*, 399, 801
- Gaztañaga E., Cabré A., Hui L., 2009, *MNRAS*, 399, 1663
- Hamana T., Colombi S. T., Thion A., Devriendt J. E. G. T., Mellier Y., Bernardeau F., 2002, *MNRAS*, 330, 365
- Heavens A., 2003, *MNRAS*, 343, 1327
- Heavens A. F., Kitching T. D., Taylor A. N., 2006, *MNRAS*, 373, 105
- Heavens A. F., Taylor A. N., 1995, *MNRAS*, 275, 483
- Hinshaw G., Nolte M. R., Bennett C. L., Bean R., Doré O., Greason M. R., Halpern M., Hill R. S., et al., 2007, *ApJS*, 170, 288
- Hinshaw G., Spergel D. N., Verde L., Hill R. S., Meyer S. S., Barnes C., Bennett C. L., Halpern M., et al., 2003, *ApJS*, 148, 135
- Hoekstra H., Jain B., 2008, *Annual Review of Nuclear and Particle Science*, 58, 99
- Hu W., 1999, *ApJL*, 522, L21
- Hu W., Sugiyama N., 1996, *ApJ*, 471, 542
- Jeong D., Komatsu E., 2006, *ApJ*, 651, 619
- Jeong D., Komatsu E., 2009, *ApJ*, 691, 569
- Jürgens G., Bartelmann M., 2012, *ArXiv e-prints* 1204.6524
- Kazin E. A., Blanton M. R., Scoccimarro R., McBride C. K., Berlind A. A., 2010, *ApJ*, 719, 1032
- Kazin E. A., Blanton M. R., Scoccimarro R., McBride C. K., Berlind A. A., Bahcall N. A., Brinkmann J., Czarapata P., et al., 2010, *ApJ*, 710, 1444
- Kitching T. D., Heavens A. F., Taylor A. N., Brown M. L., Meisenheimer K., Wolf C., Gray M. E., Bacon D. J., 2007, *MNRAS*, 376, 771
- Kitching T. D., Heavens A. F., Verde L., Serra P., Melchiorri A., 2008, *Phys. Rev. D*, 77, 103008
- Kitching T. D., Taylor A. N., Heavens A. F., 2008, *MNRAS*, 389, 173
- Krause E., Hirata C. M., 2010, *A&A*, 523, A28
- Labatie A., Starck J. L., Lachièze-Rey M., 2012, *ApJ*, 746, 172
- Lanusse F., Rassat A., Starck J.-L., 2012, *A&A*, 540, A92
- Larson D., Dunkley J., Hinshaw G., Komatsu E., Nolte M. R., Bennett C. L., Gold B., Halpern M., et al., 2011, *ApJS*, 192, 16
- Leistedt B., Rassat A., Réfrégier A., Starck J.-L., 2012, *A&A*, 540, A60
- Leonard A., Dupé F.-X., Starck J.-L., 2012, *A&A*, 539, A85
- Limber D. N., 1954, *ApJ*, 119, 655
- Linder E. V., Jenkins A., 2003, *MNRAS*, 346, 573
- Massey R., Rhodes J., Leauthaud A., Capak P., Ellis R., Koekoemoer A., Réfrégier A., Scoville N., et al., 2007, *ApJS*, 172, 239
- Matarrese S., Pietroni M., 2008, *Modern Physics Letters A*, 23, 25
- Mehta K. T., Cuesta A. J., Xu X., Eisenstein D. J., Padmanabhan N., 2012, *ArXiv e-prints* 1202.0092
- Meiksin A., White M., Peacock J. A., 1999, *MNRAS*, 304, 851
- Montanari F., Durrer R., 2011, *Phys. Rev. D*, 84, 023522
- Munshi D., Heavens A., Coles P., 2011, *MNRAS*, 411, 2161
- Munshi D., Valageas P., van Waerbeke L., Heavens A., 2008, *Physics Reports*, 462, 67
- Nishimichi T., Ohmuro H., Nakamichi M., Taruya A., Yahata K., Shirata A., Saito S., Nomura H., Yamamoto K., Suto Y., 2007, *PASJ*, 59, 1049
- Nishimichi T., Shirata A., Taruya A., Yahata K., Saito S., Suto Y., Takahashi R., Yoshida N., Matsubara T., Sugiyama N., Kayo I., Jing Y., Yoshikawa K., 2009, *PASJ*, 61, 321
- Nolte M. R., Dunkley J., Hill R. S., Hinshaw G., Komatsu E., Larson D., Page L., Spergel D. N., et al., 2009, *ApJS*, 180, 296
- Padmanabhan N., Schlegel D. J., Seljak U., Makarov A., Bahcall N. A., Blanton M. R., Brinkmann J., Eisenstein D. J., et al., 2007, *MNRAS*, 378, 852
- Padmanabhan N., Xu X., Eisenstein D. J., Scalzo R., Cuesta A. J., Mehta K. T., Kazin E., 2012, *ArXiv e-prints* 1202.0090
- Parejko J. K., Sunayama T., Padmanabhan N., Wake D. A., Berlind A. A., Bizyaev D., Blanton M., Bolton A. S., et al., 2012, *ArXiv e-prints* 1211.3976
- Parkinson D., Riemer-Sørensen S., Blake C., Poole G. B., Davis T. M., Brough S., Colless M., Contreras C., et al. 2012, *Phys. Rev. D*, 86, 103518
- Percival W. J., Burke D., Heavens A., Taylor A., Cole S., Peacock J. A., Baugh C. M., Bland-Hawthorn J., et al., 2004, *MNRAS*, 353, 1201
- Percival W. J., Cole S., Eisenstein D. J., Nichol R. C., Peacock J. A., Pope A. C., Szalay A. S., 2007, *MNRAS*, 381, 1053
- Percival W. J., Nichol R. C., Eisenstein D. J., Weinberg D. H., Fukugita M., Pope A. C., Schneider D. P., Szalay A. S., et al., 2007, *ApJ*, 657, 51
- Percival W. J., Reid B. A., Eisenstein D. J., Bahcall N. A., Budavari T., Frieman J. A., Fukugita M., Gunn J. E., et al., 2010, *MNRAS*, 401, 2148
- Pietroni M., 2008, *JCAP*, 10, 36
- Pratten G., Munshi D., 2013, *ArXiv e-prints*

- Rassat A., Refregier A., 2012, *A&A*, 540, A115
- Schneider P., van Waerbeke L., Mellier Y., 2002, *A&A*, 389, 729
- Seitz S., Schneider P., 1994, *A&A*, 287, 349
- Seitz S., Schneider P., Ehlers J., 1994, *Classical and Quantum Gravity*, 11, 2345
- Seljak U., Zaldarriaga M., 1996, *ApJ*, 469, 437
- Seo H.-J., Eisenstein D. J., 2003, *ApJ*, 598, 720
- Shapiro C., Cooray A., 2006, *Journal of Cosmology and Astro-Particle Physics*, 3, 7
- Springel V., White S. D. M., Jenkins A., Frenk C. S., Yoshida N., Gao L., Navarro J., Thacker R., et al., 2005, *Nature*, 435, 629
- Sutherland W., 2012, *MNRAS*, 426, 1280
- Takada M., Jain B., 2004, *MNRAS*, 348, 897
- Taruya A., Nishimichi T., Saito S., Hiramatsu T., 2009, *Phys. Rev. D*, 80, 123503
- Turner M. S., White M., 1997, *Phys. Rev. D*, 56, 4439
- Wang L., Steinhardt P. J., 1998, *ApJ*, 508, 483
- Wright E. L., Bennett C. L., Gorski K., Hinshaw G., Smoot G. F., 1996, *ApJL*, 464, L21
- Zhao G.-B., Saito S., Percival W. J., Ross A. J., Montesano F., Viel M., Schneider D. P., Ernst D. J., et al., 2012, *ArXiv e-prints* 1211.3741

This paper has been typeset from a $\text{\TeX}/\text{\LaTeX}$ file prepared by the author.